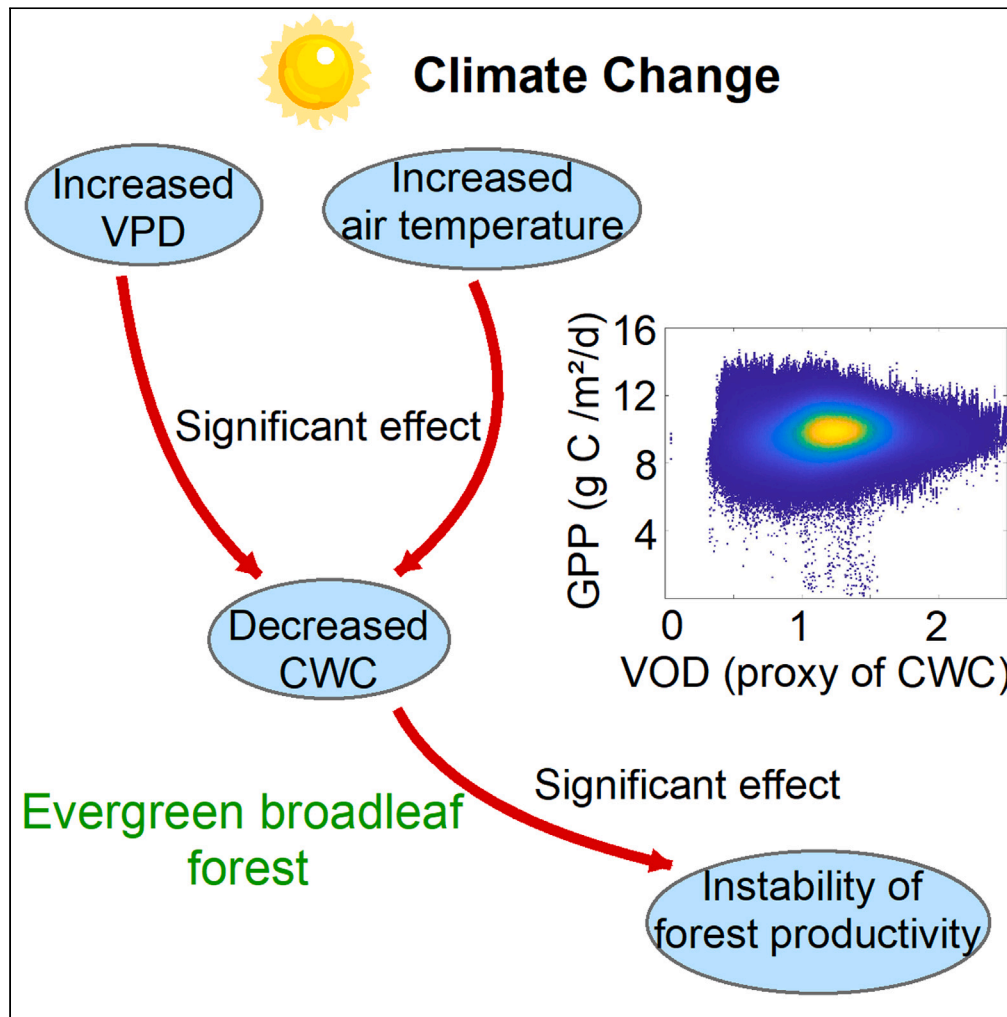**Article**

Decline in stability of forest productivity in the tropics as determined by canopy water content

Feng Liu, Hongyan Liu, Wulahati Adalibieke, ..., Siwen Feng, Liang Shi, Xinrong Zhu

lhy@urban.pku.edu.cn

Highlights

Regulation of forest canopy water on productivity stability is globally applicable

Decreasing canopy water content threatens forest productivity under climate change

Decreasing canopy water is unexpectedly observed in evergreen broadleaf forest

Article

Decline in stability of forest productivity in the tropics as determined by canopy water content

Feng Liu,[1] Hongyan Liu,[1,3,*] Wulahati Adalibieke,[1] Zhaoyu Peng,[1] Boyi Liang,[2] Siwen Feng,[1] Liang Shi,[1] and Xinrong Zhu[1]

SUMMARY

The impacts of low soil moisture (SM) and high vapour pressure deficit (VPD) on tree's photosynthesis and productivity are ultimately realized by changing water content in the canopy leaves. In this study, variations in canopy water content (CWC) that can be detected from microwave remotely sensed vegetation optical depth (VOD) have been proposed as a promising measure of vegetation water status, and we first reported that the regulation of CWC on productivity stability is universally applicable for global forests. Results of structural equation model (SEM) also confirmed the significant negative effect of CWC on coefficient of variation (CV) of productivity, indicating that the decrease in CWC could inevitably induce the instability of forest productivity under climate change. The most significant decrease ($p < 0.01$) of CWC is observed primarily in evergreen broadleaf forest in the tropics, implying an increasing instability of the most important carbon sink in terrestrial ecosystem.

INTRODUCTION

More frequent drought events and increasing water constraint have considerable impacts on forest growth and can alter global carbon-water cycles and energy exchanges.[1–3] Related studies have revealed that the worldwide vapor pressure deficit (VPD) has increased considerably since the 1990s, inducing an enhanced atmospheric water demand for forests.[4–6] In semi-arid ecosystems, warming-related drought stress may also be characterized by limited soil moisture (SM), which serves as the direct water pool for forest growth.[7–9] From the perspective of the soil-plant-atmosphere continuum (SPAC), the water availability of global forests has inevitably been constrained by changing VPD and SM.[10–12] Considering that water is fundamental in determining plant photosynthesis, vegetation water content has the direct impact on forest productivity.[13,14] However, most previous studies have focused on the roles of VPD, SM and their interaction, instead of the vegetation water content itself.[15–17]

Numerous metrics have been proposed for forest water status, ranging from the leaf-level equivalent water thickness (EWT), live fuel moisture content (LFMC), and relative water content (RWC) to the higher-level canopy water content (CWC).[18–21] In particular, CWC underpins important physiological functions (e.g. photosynthesis) and has been adopted as an indispensable representation of warming-induced disturbances in forests.[22] In contrast to *in situ* measurements with spatiotemporal limitations in data acquisition, remote sensing observations contribute to the large-scale monitoring of long-term variations in forest water status.[23,24] Widely applied optical remote sensing techniques utilize multispectral and hyperspectral indices to provide estimates of CWC.[25] However, the inherent defects of optical remote sensing could be summarized as the high sensitivity to atmospheric conditions (e.g., aerosol pollution, cloud cover, and water vapor), which used to prevent the accurate and timely acquisition of data.[26] Benefitting from relatively long wavelengths, microwave remote sensing possesses a stronger penetration capacity in the atmosphere and can thus provide valid global observations at almost daily frequencies.[27,28] Specifically, the vegetation optical depth (VOD) obtained from passive microwave observations is a dimensionless parameter that describes the attenuation rate of microwaves as they pass through the vegetation canopy.[29] Theoretical considerations and related experiments have revealed that VOD is linearly proportional to the vegetation water content, and the responses of VOD to forest water status (e.g., CWC) are primarily determined by corresponding wavelengths.[30,31] Among numerous microwave datasets,[32,33] VOD estimates from short wavelengths (e.g., the Ku-band and X-band) are more sensitive to canopy leaves, while the long wavelength VOD (typically as the L-band) generally presents

[1]College of Urban and Environmental Sciences and MOE Laboratory for Earth Surface Processes, Peking University, Beijing 100871, China

[2]College of Forestry, Precision Forestry Key Laboratory of Beijing, Beijing Forestry University, Beijing 100083, China

[3]Lead contact

*Correspondence: lhy@urban.pku.edu.cn

https://doi.org/10.1016/j.isci.2023.107211

higher sensitivity to deeper forest layers, including stems and other woody components.[20,21,34] Accordingly, short wavelength microwaves contribute to reducing the significant impacts of heterogeneous understorey cover on canopy VOD estimates, meanwhile eliminating more compensating errors from the SM contribution. All these features make short wavelength VOD a promising proxy for forest CWC assessments at regional and global scales.

In this study, we adopted the short wavelength Ku-band VOD as the proxy for forest CWC, intending to assess the regulation of CWC on forest productivity (represented by gross primary productivity, GPP) over the 1987–2017 period. The global forest types were first extracted from time-series MODIS land cover data, meanwhile eliminating the disturbances induced by land cover changes. This work continued the exploration of forest CWC in our previous studies,[35,36] further expanding the observations from single tree species at sample plots to global-scale forest vegetation. The trend analysis was then conducted with the Mann-Kendall (MK) monotonic trend test to determine the spatial and temporal patterns of CWC variation trends within each forest type. Finally, the impacts of CWC on the stability of forest GPP (represented by coefficient of variation, CV) were quantified with weighted linear regression and structural equation model (SEM). We adopted forest CWC as a starting point to assess the regulation of water content on the stability of forest productivity, contributing to the comprehensive understanding of forest carbon sinks in the context of future climate change.
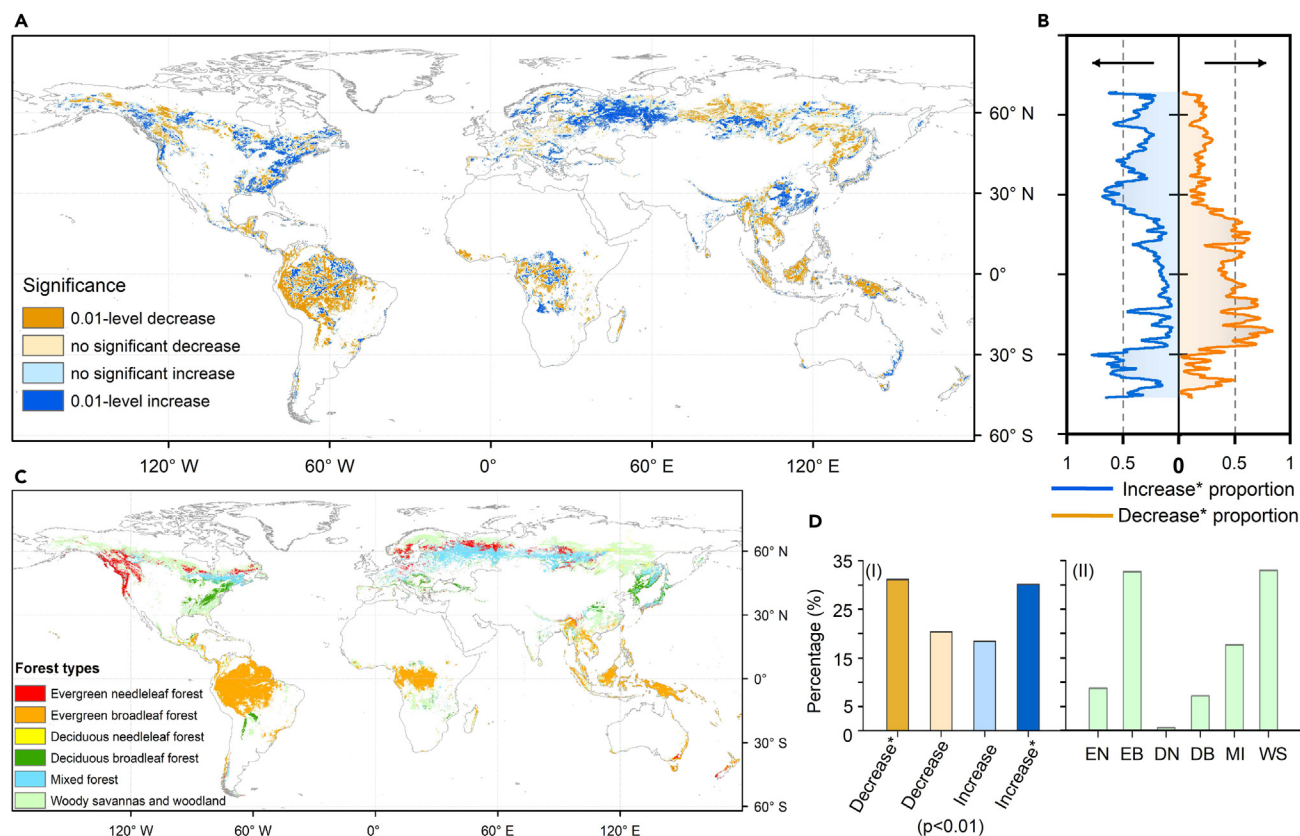
RESULTS

Spatial and temporal patterns of VOD variation trends in global forests

The results of the MK test exhibited obvious spatial heterogeneity, reflecting distinguished VOD dynamics among the various forest types (Figure 1A). In terms of latitudinal zonality, forests with significant increases in VOD occupied as low as 6% at low latitudes and higher than 50% at middle-high latitudes, respectively (Figure 1B). In particular, regions with significant increases in VOD at high latitudes in the Northern Hemisphere primarily corresponded to mixed forest. In contrast, significant decreases in VOD were in the majority in low-latitude forests, and the proportion could reach 86% at most. Within the decreasing-VOD dominated regions at low latitudes, especially around the equator, the area of evergreen broadleaf forest was the largest. Overall, more than 60% of the global forest presented significant variation trends of VOD over the past 30 years, and the proportion of 0.01-level decreases (31.14%) was slightly higher than that of 0.01-level increases (30.11%) (Figures 1D–1I). For the distributions of the six forest types (Table S1), large differences in area were observed (Figure 1C). Specifically, evergreen broadleaf forest (EB), woody savannas and woodland (WS) occupy the highest proportions, accounting for more than 32% of global forests each (Figures 1D–1I).

Considering the distinguished responses of global forests to climate change, the averaged VOD anomaly time series within each forest type was calculated at a monthly scale. In particular, the VOD anomaly of evergreen needleleaf forest generally presented continuous increases over the entire study period, with a peak in 2011 (Figure 2A). In contrast, the VOD anomaly of evergreen broadleaf forest exhibited an overall decreasing trend, which was the only case among all forest types (Figure 2B). Especially after 2009, the values were much lower than the multi-year average of the past decades. In addition, the sliding-window (15 years) MK test on the VOD anomaly time series of all pixels within each forest type also indicated that VOD of evergreen broadleaf forest exhibited the most significant decrease around the globe (Figure S1B). In terms of deciduous needleleaf forest (Figure 2C), relatively large interannual variations in VOD were observed, possibly owing to the limited amount of data (only 0.62% of global forests, 7314 pixels) induced by the sparser distribution. The VOD anomaly of deciduous broadleaf forest (Figure 2D) and woody savannas and woodland (Figure 2F) basically exhibited long-term stability with no continuous increases or decreases. Last, the mixed forest possessed a trend of increasing VOD anomaly, similar to that of the evergreen needleleaf forest, which peaked in 2009 (Figure 2E). The results confirmed the differentiated VOD variation trends among the six types, meanwhile reflecting the ever-changing forest water status in the past decades.

Similarly, the spatial and temporal patterns of GPP variation trends in global forests were analyzed. In terms of the spatial heterogeneity, 0.01-level decreases (25.76%) and 0.01-level increases (29.42%) accounted for about 55% of GPP variations (Figure S2). The averaged anomaly time series of GLASS-GPP calculated from light use efficiency (LUE) models (Figure S3) and NIR-GPP retrieved from near-infrared remote sensing observations (Figure S4) both presented increasing instability in evergreen broadleaf forest, especially for the

Figure 1. Variation trends of the Ku-band VOD over global forests between 1987 and 2017

(A–D) The results of the MK test on the VOD time series (A) were conducted at a 99% significance level. The proportions of significant increases (increases*) and significant decreases (decreases*) (B) were computed for each latitude at increments of 0.05°. The global distributions of six forest types (C) were based on MODIS land cover data. The impacts of land cover change in the past decades were eliminated with the change detection of the time-series land cover data, and only unchanged forest areas were maintained. The proportions of distinguished VOD trends (D-I) and the proportions of six forest types (D-II) were both computed over global forests. EN, evergreen needleleaf forest; EB, evergreen broadleaf forest; DN, deciduous needleleaf forest; DB, deciduous broadleaf forest; MI, mixed forest; WS, woody savannas and woodland.

variations of GLASS-GPP (Figure S3B), which possessed the most obvious decreases throughout the 21st century and call for more attention in further study.

Regulation of VOD on the stability of forest GPP

The determination of forest water status on interannual stability of productivity was embodied in the regulating effect of CWC. Specifically, compared with annual averages, forest carbon sequestration capacity could be well presented in the annual maximum values (peak values) of VOD and GPP, which were served as the proxies for forest CWC and productivity, respectively.

Scatterplots with a 31-year (1987–2017) VOD and GLASS-GPP were generated for each forest type (Figure 3), exhibiting the fluctuation in GPP with the variation in VOD values. It is worth noting that the scatterplots corresponded to the substitution of space for time, and the temporal variation of forest CWC was represented by the values of VOD in the x axis. Particularly, instead of calculating commonly used standard deviation (SD), which required the mean values of the compared populations to be equal, the interannual variation of GPP values was expressed with CV in this study. For evergreen forest, the distributions of GPP values in both needleleaf (Figure 3[A1]) and broadleaf (Figure 3[B1]) types became increasingly concentrated as VOD increased. Based on the scatter density of GPP data, weighted linear regression of the CV$_{GPP}$ was further conducted, indicating that higher VOD values of evergreen forest corresponded to more stable productivity (Figure 3[A2, B2]). In particular, evergreen broadleaf forest possessed the highest values of VOD in global forests (Figure 3[B1]), and the R^2 (0.82) of the CV$_{GPP}$ fitting line exceeding those of
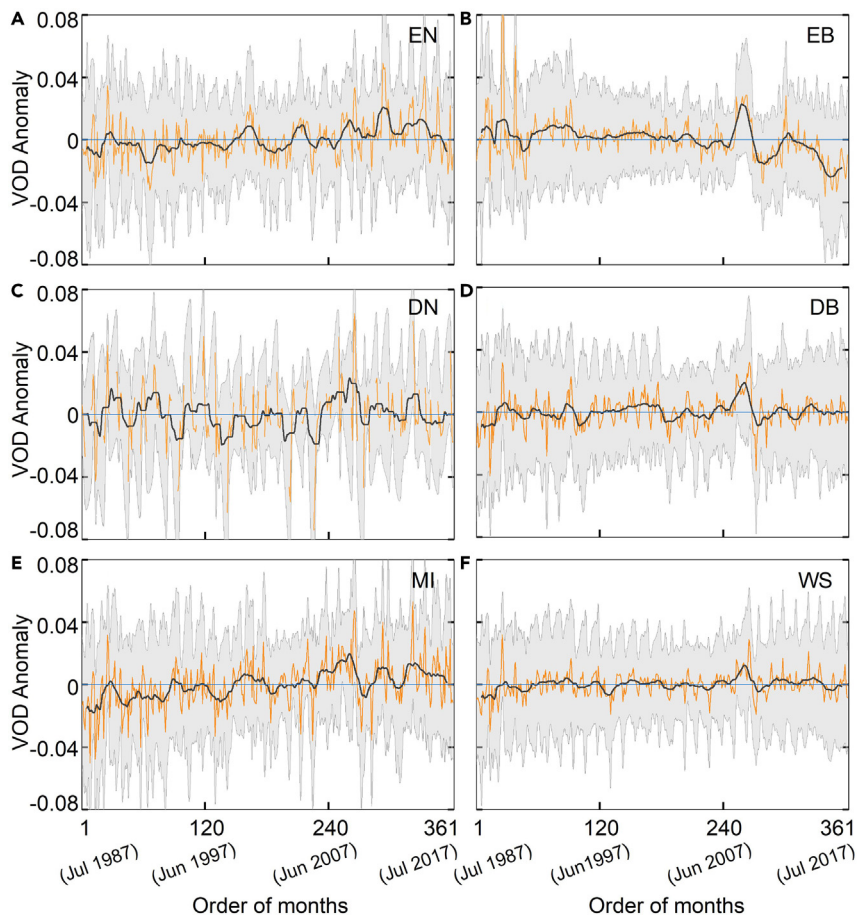
Figure 2. Globally averaged Ku-band VOD anomaly time series within six forest types

The orange lines represent the averaged values of the monthly anomaly within each forest type, and the black lines represent the results filtered by the moving average method. The gray shaded area indicates ±1 standard deviation (SD). EN, evergreen needleleaf forest; EB, evergreen broadleaf forest; DN, deciduous needleleaf forest; DB, deciduous broadleaf forest; MI, mixed forest; WS, woody savannas and woodland.

other forest types. The regulating effect of the VOD in deciduous forest was consistent with that in evergreen forest (Figure 3[C2, D2]), although deciduous needleleaf type corresponded to the minimum number of pixels in global forests. The scatter distribution of mixed forest (Figure 3[E1]) was remarkably close to that of evergreen needleleaf forest, likely owing to the similarity of dominant forest types. Last, despite the impacts of grassland in woody savannas, the regulation of VOD on the stability of GPP was still significant, and R^2 of the CV_{GPP} fitting line reached the second largest value (0.77) of all forest types (Figure 3[F2]).

Additionally, considering the impacts of leaf area index (LAI) on both VOD and GPP, their correlation in Figure 3 may arise from collinearity with LAI, rather than the regulation of water content on GPP. The scatterplots with LAI and GPP were subsequently generated, and the regulating effect of LAI on the stability of GPP was not observed, except for the positive correlation between them (Figure S5). Hence, as shown in all forest types in Figure 3, large number of GPP values were concentrated in the range from approximately 7 to 10 (g C/m^2/d), and the CV_{GPP} values presented downwards trends with increasing VOD, reflecting the determination of VOD on the stability of GPP. Furthermore, the second product of GPP estimates (NIR-GPP) also yielded similar results, confirming the robustness of the previous conclusions (Figure S6). We generated the scatterplots of VOD and GPP with different spatial resolutions (0.25 or 0.05°), different calculations of annual value (annual average or annual maximum values) and different processing modes of land cover data (land cover changes were eliminated or not eliminated). The results indicated that the relationship between VOD and the stability of GPP would not be impacted by the calculation and processing methods of input datasets (Figure S7).
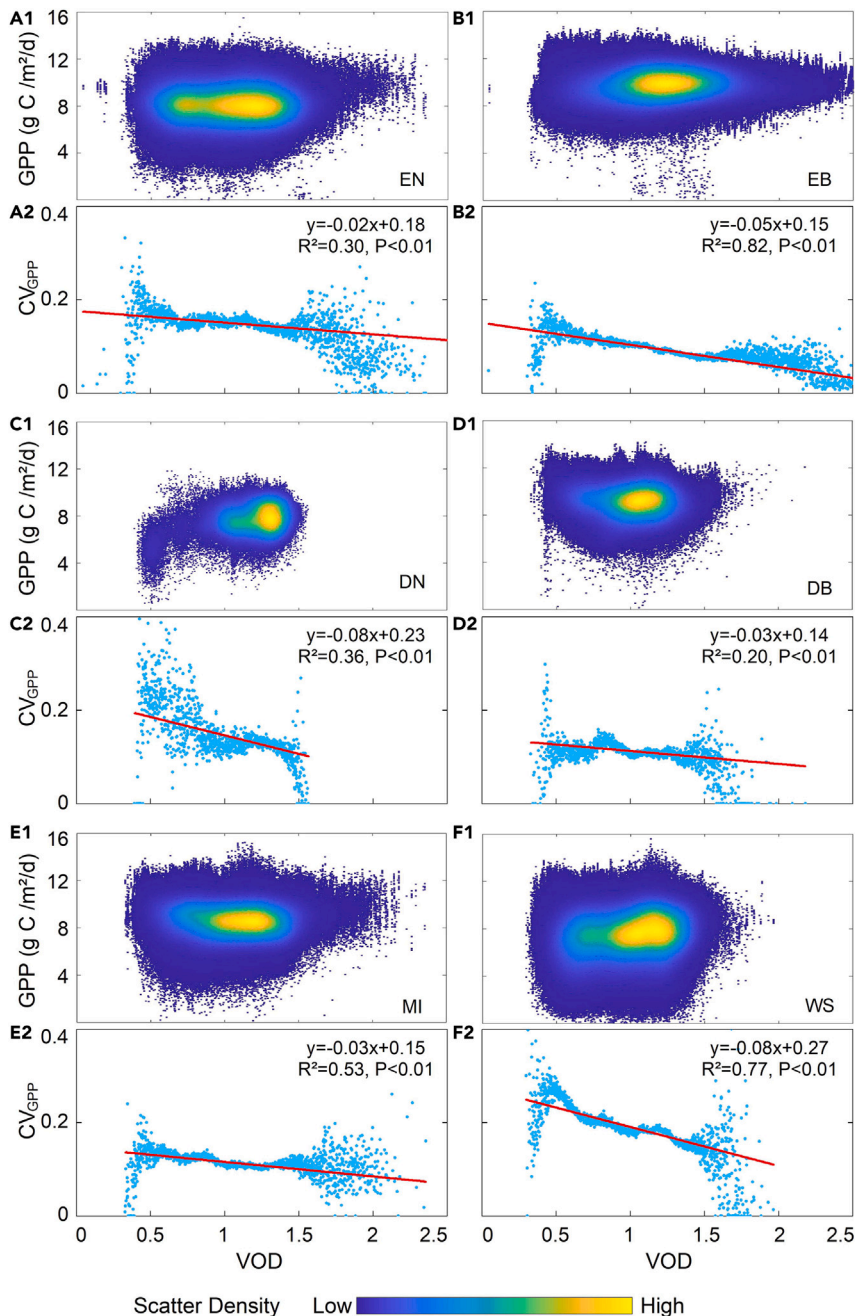
Figure 3. The regulation of VOD on the stability of GPP over global forests

Each scatterplot of VOD and GPP (A1-F1) contained 31-year data for 1987 to 2017. Considering the 0.05-degree spatial resolution, all six forest types, including evergreen needleleaf forest (EN, 103494 pixels), evergreen broadleaf forest (EB, 387273 pixels), deciduous needleleaf forest (DN, 7314 pixels), deciduous broadleaf forest (DB, 85319 pixels), mixed forest (MI, 209384 pixels), woody savannas and woodland (WS, 390018 pixels), possessed large raster data. The scatter density directly reflected that the distributions of GPP and VOD values within each forest type were very uneven, concentrating in certain value ranges. CV_{GPP} quantified the interannual variation of GPP values with the variation in VOD. The weighted linear regressions of CV_{GPP} (A2-F2) were conducted at a 99% significance level.

Effect pathways of the variables on forest productivity

SEM confirmed the dominant role of CWC (represented by VOD) in determining the stability of forest GPP, meanwhile clarifying the indirect contributions of environmental variables. We fitted pathways for all the
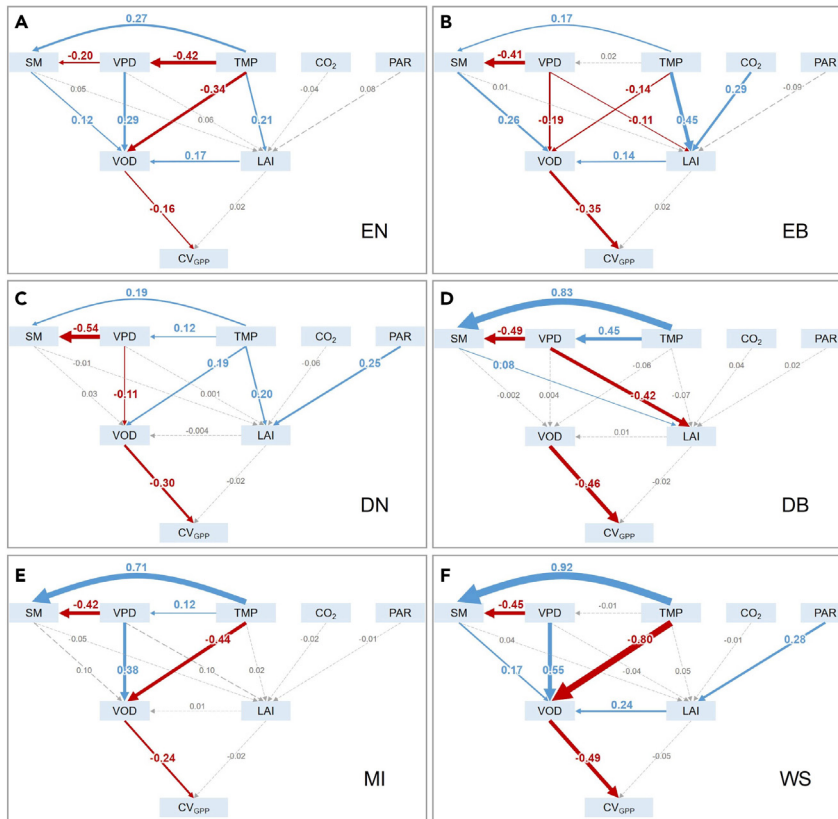
Figure 4. The results of SEM for six forest types

The established SEM for (A) evergreen needleleaf forest (p = 0.777, AIC = 96.505, BIC = 318.269, Fisher's C = 0.505), (B) evergreen broadleaf forest (p = 0.291, AIC = 98.466, BIC = 330.348, Fisher's C = 2.466), (C) deciduous needleleaf forest (p = 0.242, AIC = 98.835, BIC = 320.599, Fisher's C = 2.835), (D) deciduous broadleaf forest (p = 0.092, AIC = 100.772, BIC = 369.615, Fisher's C = 4.772), (E) mixed forest (p = 0.058, AIC = 101.689, BIC = 323.453, Fisher's C = 5.689) and (F) woody savannas and woodland (p = 0.859, AIC = 96.305, BIC = 318.069, Fisher's C = 0.305). The solid lines represent the significant effect pathways (p <0.01), and the dotted lines represent the pathways that fail to pass the significance test. The blue and red lines represent the positive effect pathways and negative effect pathways, respectively. EN, evergreen needleleaf forest; EB, evergreen broadleaf forest; DN, deciduous needleleaf forest; DB, deciduous broadleaf forest; MI, mixed forest; WS, woody savannas and woodland. SM, soil moisture; VPD, vapor pressure deficit; TMP, temperature; PAR, photosynthesis active radiation; VOD, vegetation optical depth; LAI, leaf area index; CV, coefficient of variation.

variables that directly or indirectly affected productivity, and all the final models of the six forest types passed the statistical test (p >0.05) (Figure 4).

The obtained SEM consisted of a three-layer structure, and VOD with LAI in the middle layer were the core variables connecting the environmental variables (SM, VPD, TMP, CO_2, PAR) from the top layer and productivity-related variables (CV_{GPP}) in the bottom layer. More precisely, two main effect pathways were centered on VOD and LAI. On the one hand, the pathway containing environmental variables and VOD reflected the effects of climate change on forest water status, which was actually embodied in the transpiration of the canopy. On the other hand, LAI was a proxy of canopy greenness, and the pathway containing environmental variables and LAI corresponded to the affected photosynthesis of the forest canopy. Hydraulic characteristics of the six forest types were well presented in the different effect pathways of VPD on VOD, especially the only case in evergreen broadleaf forest, where significant negative effects of TMP (−0.14) and VPD (−0.19) on VOD were observed simultaneously (Figure 4B), exactly corresponding to the most significant decreasing trend of VOD. In contrast, the results of SEM presented consistent effect pathways of the environmental variables on greenness-related LAI, despite the distinguished intensity. For each significant pathway, SM, TMP, CO_2, and PAR possessed positive effects on LAI, while only VPD corresponded to a negative effect.

The significant negative effect (p <0.01) of VOD on CV_{GPP} (from −0.16 to −0.49 in six forest types) and non-significant effect of LAI on CV_{GPP} were universally applicable (Figures 4A–4F). Particularly, VOD of woody savannas and woodland possessed the greatest negative effect (−0.49) on CV_{GPP} despite the interference of grassland (Figure 4F). In conclusion, SEM confirmed the significant effects of rising air temperature and VPD on VOD, and VOD further possessed the significant negative effect on CV_{GPP}, indicating that the decrease in VOD could inevitably induce the instability of forest productivity under climate change.

DISCUSSION

Our results revealed that the forest CWC (represented by VOD) was not completely stable on the interannual scale. For the temporal patterns, differing from the commonly recognized seasonal VOD anomaly,[26,28] the interannual fluctuations in VOD could significantly threaten forest productivity in some areas. For the spatial patterns of the ever-changing VOD, the typical and continuous increases were presented in evergreen needleleaf forest and mixed forest, while evergreen broadleaf forest possessed the most significant decreasing trend. Some previous studies have focused on forest growth in the context of water deficits in both the atmosphere and soil,[5,14,35] but the scaling up from specific areas to global forest ecosystems is still needed. Owing to the spatial heterogeneity of global VPD and SM, variations in CWC in the six forest types responded inconsistently to climate change. Specifically, the CWC of evergreen needleleaf forest presented continuous increases, and there was no sign of canopy water deficit in this area. A related study has also suggested that gymnosperms have higher hydraulic safety margins than angiosperms, reflecting higher tolerance to drought stress and a lower likelihood of hydraulic failure.[46] The CWC of evergreen broadleaf forest exhibited a continuous and significant decreasing trend in our results, which indicated its higher vulnerability to climate change from the perspective of water stress.[47,48] In contrast, the CWC of mixed forest possessed an overall increasing trend for the entire study period, probably owing to a certain proportion of evergreen needleleaf trees therein, also reflecting the contribution of higher forest-type diversity in reducing the adverse effects of climate change in vast boreal forests.[49]

There was a high probability for the dynamic balance of forest CWC to be disrupted by the enhanced atmospheric water demand under climate change. Related studies have revealed that the global averaged VPD exhibited a slight increase before the late 1990s, after which, especially throughout the 21st century, a sharp increase was observed based on multiple climate datasets.[4,6] Correspondingly, the decadal variation trends of CWC in evergreen needleleaf forest, mixed forest, and evergreen broadleaf forest were generally marked by a transition around the 2010s. Hence, the persistent and widespread increase in VPD could be considered a major driving factor in the variations in forest CWC. A higher VPD indicates a stronger atmospheric water demand, which could alter land evapotranspiration in global forests primarily through the transpiration of the canopy. Transpiration pull used to be considered the primary impetus of water uptake from roots, transporting almost 97% of water to the atmosphere in a gaseous form.[50] Besides, the hydraulic architecture of each forest type also has considerable impact on the long-term variation trends of CWC.[51,52] Water in the forest canopy is always in a state of dynamic change while the overall trend is relatively stable. However, for the most surprising situation, the CWC of evergreen broadleaf forest failed to remain stable against global warming, consequently exhibiting a decreasing trend in the past decades. Water stored in the canopy enables physiological and biochemical functions, such as maintaining the normal process of photosynthesis.[19,53] A previous study indicated that CWC may decrease at first during a drought period, and sustained water deficit may in turn induce an accompanying reduction in canopy greenness,[36] so the stability of CWC determines the stability of photosynthetic assimilation. Rising air temperatures and the accompanying increase in evapotranspiration rates are predicted for the forthcoming years,[4,5] which would bring greater uncertainty to the variations in forest CWC.

Our results further suggested that the regulating effect of CWC on the stability of GPP was universally applicable for global forests, and higher CWC values generally corresponded to more stable GPP within each forest type. In other words, the decrease in CWC could inevitably induce the instability of forest productivity, particularly in evergreen broadleaf forest that used to be the largest contributor to terrestrial productivity.[54,55] Owing to the impacts of high cloud cover and rainy weather on the quality of optical remote sensing observations, especially the satellite-based LAI and PAR, there are large uncertainties in the estimates of forest productivity over tropical areas, consequently inducing discrepancies among different GPP products.[40] However, quite a few studies, including all-weather microwave monitoring, showed that the decrease in global forest productivity occurred primarily in evergreen broadleaf forest, especially in the Amazon.[56,57] In contrast to other types, the productivity of evergreen broadleaf forest

exhibited a decreasing trend from the 1980s and went below the average throughout the 21st century.[48] Hence, the continuous decrease in CWC in evergreen broadleaf forest resulted in less stable GPP, which presented a downwards trend, reflecting the nonnegligible risks under climate change. Evergreen needleleaf forest and mixed forest exhibited continuous increases in CWC during the entire study period, indicating more stable GPP in the forthcoming years, which could serve as the stabilizer of global forest productivity.[48] Relatively large interannual variations of CWC were observed in deciduous needleleaf forest, and related studies also indicated that deciduous needleleaf forest was one of the most sensitive biomes to temperature and exhibited larger interannual variations.[58] Considering the complicated response of deciduous needleleaf forest to climate change, more attention is needed in further studies.

Limitations of the study

Our results are subject to some limitations. First, the mechanism study of adopting Ku-band VOD as the proxy for forest CWC needs to be strengthened. Remote sensing products from rest microwave bands (e.g., the C-band and X-band) or other effective proxy indicators of CWC from multi-source datasets need to be explored. Second, in order to eliminate redundant elements, the research objects are determined as six forest types based on land cover data. However, considering the wide variation and spatial heterogeneity across pixels within each forest type, further studies could be more precise and targeted with differentiating the confounding impacts of biomass, climatic and hydrological conditions. Third, it would be more persuasive to conduct field validation for the remotely sensed relationship between CWC and forest productivity. There is a huge spatial-scale difference between VOD products (resolution of 0.25°) and traditional field investigation in ecological research. Hence, the practical problems of scale difference and data limitation should be resolved in the validation.

Conclusions

In summary, our results indicated that the regulation of CWC on the stability of productivity was universally applicable for global forests, and higher CWC values corresponded to more stable productivity. In particular, the CWC of evergreen broadleaf forest possessed the most significant decreasing trend in the six forest types. However, as the largest contributor to terrestrial productivity, the decreasing CWC and productivity of evergreen broadleaf forest call for more attention in the context of climate change.

STAR★METHODS

Detailed methods are provided in the online version of this paper and include the following:

- KEY RESOURCES TABLE
- RESOURCE AVAILABILITY
  - Lead contact
  - Materials availability
  - Data and code availability
- METHOD DETAILS
  - Forest cover extraction
  - VOD processing
  - GPP and LAI processing
  - Temperature and VPD processing
  - SM and PAR processing
  - Acquisition of CO_2 concentration
  - Conduction of MK test
  - Construction of SEM

SUPPLEMENTAL INFORMATION

Supplemental information can be found online at https://doi.org/10.1016/j.isci.2023.107211.

AUTHOR CONTRIBUTIONS

Conceptualization: F.L., and H.L.; Methodology: F.L., H.L., W.A., B.L., S.F., and L.S.; Investigation: F.L., H.L., Z.P., and X.Z.; Visualization: F.L., W.A., and Z.P.; Project administration: H.L.; Supervision: H.L.; Writing – original draft: F.L., H.L., W.A., and Z.P.; Writing – review & editing: F.L., H.L., and B.L.

DECLARATION OF INTERESTS

REFERENCES

1. Anderegg, W.R.L., Konings, A.G., Trugman, A.T., Yu, K., Bowling, D.R., Gabbitas, R., Karp, D.S., Pacala, S., Sperry, J.S., Sulman, B.N., and Zenes, N. (2018). Hydraulic diversity of forests regulates ecosystem resilience during drought. Nature 561, 538–541.

2. IPCC (2021). In Climate Change 2021: The Physical Science Basis. Contribution of Working Group I to the Sixth Assessment Report of the Intergovernmental Panel on Climate Change, V. Masson-Delmotte, P. Zhai, A. Pirani, S.L. Connors, C. Péan, S. Berger, N. Caud, Y. Chen, L. Goldfarb, and M.I. Gomis, et al., eds. (Cambridge University Press) In Press.

3. Jiao, W., Wang, L., Smith, W.K., Chang, Q., Wang, H., and D' Odorico, P. (2021). Observed increasing water constraint on vegetation growth over the last three decades. Nat. Commun. 12, 3777.

4. Grossiord, C., Buckley, T.N., Cernusak, L.A., Novick, K.A., Poulter, B., Siegwolf, R.T.W., Sperry, J.S., and McDowell, N.G. (2020). Plant responses to rising vapor pressure deficit. New Phytol. 226, 1550–1566.

5. Restaino, C.M., Peterson, D.L., and Littell, J. (2016). Increased water deficit decreases Douglas fir growth throughout western US forests. Proc. Natl. Acad. Sci. USA 113, 9557–9562.

6. Yuan, W., Zheng, Y., Piao, S., Ciais, P., Lombardozzi, D., Wang, Y., Ryu, Y., Chen, G., Dong, W., Hu, Z., et al. (2019). Increased atmospheric vapor pressure deficit reduces global vegetation growth. Sci. Adv. 5, eaax1396.

7. Green, J.K., Seneviratne, S.I., Berg, A.M., Findell, K.L., Hagemann, S., Lawrence, D.M., and Gentine, P. (2019). Large influence of soil moisture on long-term terrestrial carbon uptake. Nature 565, 476–479.

8. Liu, L., Gudmundsson, L., Hauser, M., Qin, D., Li, S., and Seneviratne, S.I. (2020). Soil moisture dominates dryness stress on ecosystem production globally. Nat. Commun. 11, 4892.

9. Stocker, B.D., Zscheischler, J., Keenan, T.F., Prentice, I.C., Peñuelas, J., and Seneviratne, S.I. (2018). Quantifying soil moisture impacts on light use efficiency across biomes. New Phytol. 218, 1430–1449.

10. Goldsmith, G.R. (2013). Changing directions: the atmosphere-plant-soil continuum. New Phytol. 199, 4–6.

11. Novick, K.A., Ficklin, D.L., Stoy, P.C., Williams, C.A., Bohrer, G., Oishi, A., Papuga, S.A., Blanken, P.D., Noormets, A., Sulman, B.N., et al. (2016). The increasing importance of atmospheric demand for ecosystem water and carbon fluxes. Nat. Clim. Change 6, 1023–1027.

12. Rogers, A., Medlyn, B.E., Dukes, J.S., Bonan, G., von Caemmerer, S., Dietze, M.C., Kattge, J., Leakey, A.D.B., Mercado, L.M., Niinemets, Ü., et al. (2017). A roadmap for improving the representation of photosynthesis in Earth system models. New Phytol. 213, 22–42.

13. Buermann, W., Forkel, M., O'Sullivan, M., Sitch, S., Friedlingstein, P., Haverd, V., Jain, A.K., Kato, E., Kautz, M., Lienert, S., et al. (2018). Widespread seasonal compensation effects of spring warming on northern plant productivity. Nature 562, 110–114.

14. Dannenberg, M.P., Wise, E.K., and Smith, W.K. (2019). Reduced tree growth in the semiarid United States due to asymmetric responses to intensifying precipitation extremes. Sci. Adv. 5, eaaw0667.

15. Babst, F., Bouriaud, O., Poulter, B., Trouet, V., Girardin, M.P., and Frank, D.C. (2019). Twentieth century redistribution in climatic drivers of global tree growth. Sci. Adv. 5, eaat4313.

16. Jung, M., Reichstein, M., Schwalm, C.R., Huntingford, C., Sitch, S., Ahlström, A., Arneth, A., Camps-Valls, G., Ciais, P., Friedlingstein, P., et al. (2017). Compensatory water effects link yearly global land CO_2 sink changes to temperature. Nature 541, 516–520.

17. Lian, X., Piao, S., Chen, A., Huntingford, C., Fu, B., Li, L.Z.X., Huang, J., Sheffield, J., Berg, A.M., Keenan, T.F., et al. (2021). Multifaceted characteristics of dryland aridity changes in a warming world. Nat. Rev. Earth Environ. 2, 232–250.

18. Asner, G.P., Brodrick, P.G., Anderson, C.B., Vaughn, N., Knapp, D.E., and Martin, R.E. (2016). Progressive forest canopy water loss during the 2012-2015 California drought. Proc. Natl. Acad. Sci. USA 113, E249–E255.

19. Elsherif, A., Gaulton, R., Shenkin, A., Malhi, Y., and Mills, J. (2019). Three dimensional mapping of forest canopy equivalent water thickness using dual-wavelength terrestrial laser scanning. Agric. For. Meteorol. 276–277, 107627.

20. Fan, L., Wigneron, J.P., Xiao, Q., Al-Yaari, A., Wen, J., Martin-StPaul, N., Dupuy, J.L., Pimont, F., Al Bitar, A., Fernandez-Moran, R., and Kerr, Y.H. (2018). Evaluation of microwave remote sensing for monitoring live fuel moisture content in the Mediterranean region. Remote Sens. Environ. 205, 210–223.

21. Momen, M., Wood, J.D., Novick, K.A., Pangle, R., Pockman, W.T., McDowell, N.G., and Konings, A.G. (2017). Interacting effects of leaf water potential and biomass on vegetation optical depth. J. Geophys. Res. Biogeosci. 122, 3031–3046.

22. Asner, G.P., Nepstad, D., Cardinot, G., and Ray, D. (2004). Drought stress and carbon uptake in an Amazon forest measured with spaceborne imaging spectroscopy. Proc. Natl. Acad. Sci. USA 101, 6039–6044.

23. Anderegg, W.R.L., Trugman, A.T., Badgley, G., Konings, A.G., and Shaw, J. (2020). Divergent forest sensitivity to repeated extreme droughts. Nat. Clim. Change 10, 1091–1095.

24. Huang, C.Y., Anderegg, W.R.L., and Asner, G.P. (2019). Remote Sensing of Forest Die-Off in the Anthropocene: From Plant Ecophysiology to Canopy Structure (Remote Sensing of Environment), p. 231.

25. Colombo, R., Meroni, M., Marchesi, A., Busetto, L., Rossini, M., Giardino, C., and Panigada, C. (2008). Estimation of leaf and canopy water content in poplar plantations by means of hyperspectral indices and inverse modeling. Remote Sens. Environ. 112, 1820–1834.

26. Tian, F., Brandt, M., Liu, Y.Y., Verger, A., Tagesson, T., Diouf, A.A., Rasmussen, K., Mbow, C., Wang, Y., and Fensholt, R. (2016).

Remote sensing of vegetation dynamics in drylands: Evaluating vegetation optical depth (VOD) using AVHRR NDVI and in situ green biomass data over West African Sahel. Remote Sens. Environ. *177*, 265–276.

27. Li, R., Wang, Y., Hu, J., Wang, Y., Min, Q., Bergeron, Y., Valeria, O., Gao, Z., Liu, J., and Fu, Y. (2020). Spatiotemporal variations of satellite microwave emissivity difference vegetation index in China under clear and cloudy skies. Earth Space Sci. *7*.

28. Tian, F., Wigneron, J.-P., Ciais, P., Chave, J., Ogée, J., Peñuelas, J., Ræbild, A., Domec, J.-C., Tong, X., Brandt, M., et al. (2018). Coupling of ecosystem-scale plant water storage and leaf phenology observed by satellite. Nat. Ecol. Evol. *2*, 1428–1435.

29. Konings, A.G., Rao, K., and Steele-Dunne, S.C. (2019). Macro to micro: microwave remote sensing of plant water content for physiology and ecology. New Phytol. *223*, 1166–1172.

30. Frappart, F., Wigneron, J.-P., Li, X., Liu, X., Al-Yaari, A., Fan, L., Wang, M., Moisy, C., Le Masson, E., Aoulad Lafkih, Z., et al. (2020). Global Monitoring of the Vegetation Dynamics from the Vegetation Optical Depth (VOD): A Review. Rem. Sens. *12*, 2915.

31. Jackson, T.J., and Schmugge, T.J. (1991). Vegetation effects on the microwave emission of soils. Remote Sens. Environ. *36*, 203–212.

32. Li, X., Wigneron, J.-P., Frappart, F., Fan, L., Ciais, P., Fensholt, R., Entekhabi, D., Brandt, M., Konings, A.G., Liu, X., et al. (2021). Global-scale assessment and inter-comparison of recently developed/reprocessed microwave satellite vegetation optical depth products. Remote Sens. Environ. *253*, 112208.

33. Wigneron, J.-P., Li, X.J., Frappart, F., Fan, L., Al-Yaari, A., De Lannoy, G., Liu, X.Z., Wang, M.J., Le Masson, E., and Moisy, C. (2021). SMOS-IC Data Record of Soil Moisture and L-VOD: Historical Development, Applications and Perspectives (Remote Sensing of Environment), p. 254.

34. Konings, A.G., and Gentine, P. (2017). Global variations in ecosystem-scale isohydricity. Global Change Biol. *23*, 891–905.

35. Liu, F., Liu, H., Xu, C., Zhu, X., He, W., and Qi, Y. (2021). Remotely sensed birch forest resilience against climate change in the northern China forest-steppe ecotone. Ecol. Indicat. *125*, 107526.

36. Liu, F., Liu, H., Xu, C., Shi, L., Zhu, X., Qi, Y., and He, W. (2021). Old-growth forests show low canopy resilience to droughts at the southern edge of the taiga. Global Change Biol. *27*, 2392–2402.

37. Moesinger, L., Dorigo, W., de Jeu, R., van der Schalie, R., Scanlon, T., Teubner, I., and Forkel, M. (2020). The global long-term microwave Vegetation Optical Depth Climate Archive (VODCA). Earth Syst. Sci. Data *12*, 177–196.

38. Yu, T., Sun, R., Xiao, Z., Zhang, Q., Liu, G., Cui, T., and Wang, J. (2018). Estimation of global vegetation productivity from Global LAnd Surface Satellite Data. Rem. Sens. *10*, 327.

39. Yuan, W., Liu, S., Yu, G., Bonnefond, J.M., Chen, J., Davis, K., Desai, A.R., Goldstein, A.H., Gianelle, D., Rossi, F., et al. (2010). Global estimates of evapotranspiration and gross primary production based on MODIS and global meteorology data. Remote Sens. Environ. *114*, 1416–1431.

40. Wang, S.H., Zhang, Y.G., Ju, W.M., Qiu, B., and Zhang, Z.Y. (2021). Tracking the Seasonal and Inter-annual Variations of Global Gross Primary Production during Last Four Decades Using Satellite Near-Infrared Reflectance Data (Science of the Total Environment), p. 755.

41. Buck, A.L. (1981). New equations for computing vapor pressure and enhancement factor. J. Appl. Meteorol. *20*, 1527–1532.

42. Kendall, M.G. (1975). Rank Correlation Methods (Charles Griffin).

43. Some'e, B.S., Ezani, A., and Tabari, H. (2012). Spatiotemporal trends and change point of precipitation in Iran. Atmos. Res. *113*, 1–12.

44. Gilbert, R.O. (1987). Statistical Methods for Environmental Pollution Monitoring (Van Nostrand Reinhold).

45. Grace, J.B., and Irvine, K.M. (2020). Scientist's guide to developing explanatory statistical models using causal analysis principles. Ecology *101*, e02962.

46. DeSoto, L., Cailleret, M., Sterck, F., Jansen, S., Kramer, K., Robert, E.M.R., Aakala, T., Amoroso, M.M., Bigler, C., Camarero, J.J., et al. (2020). Low growth resilience to drought is related to future mortality risk in trees. Nat. Commun. *11*, 545.

47. Mau, A., Reed, S., Wood, T., and Cavaleri, M. (2018). Temperate and tropical forest canopies are already functioning beyond their thermal thresholds for photosynthesis. Forests *9*, 47.

48. Wang, J., Sun, R., Zhang, H., Xiao, Z., Zhu, A., Wang, M., Yu, T., and Xiang, K. (2021). New global MuSyQ GPP/NPP remote sensing products from 1981 to 2018. IEEE J. Sel. Top. Appl. Earth Obs. Rem. Sens. *14*, 5596–5612.

49. Hisano, M., Chen, H.Y.H., Searle, E.B., and Reich, P.B. (2019). Species-rich boreal forests grew more and suffered less mortality than species-poor forests under the environmental change of the past half-century. Ecol. Lett. *22*, 999–1008.

50. Taiz, L., and Zeiger, E. (2010). Plant Physiology, 5th Edition (Sinauer Associates, Inc.).

51. Choat, B., Jansen, S., Brodribb, T.J., Cochard, H., Delzon, S., Bhaskar, R., Bucci, S.J., Feild, T.S., Gleason, S.M., Hacke, U.G., et al. (2012). Global convergence in the vulnerability of forests to drought. Nature *491*, 752–755.

52. Cruiziat, P., Cochard, H., and Ameglio, T. (2002). Hydraulic architecture of trees: main concepts and results. Ann. For. Sci. *59*, 723–752.

53. Lisar, S.Y.S., Motafakkerazad, R., Hossain, M.M., and Rahman, I.M.M. (2012). Water Stress in Plants: Causes, Effects and Responses. Water Stress (InTech).

54. Liu, L., Chen, X., Ciais, P., Yuan, W., Maignan, F., Wu, J., Piao, S., Wang, Y.P., Wigneron, J.P., Fan, L., et al. (2022). Tropical tall forests are more sensitive and vulnerable to drought than short forests. Global Change Biol. *28*, 1583–1595.

55. Qin, Y., Xiao, X., Wigneron, J.-P., Ciais, P., Brandt, M., Fan, L., Li, X., Crowell, S., Wu, X., Doughty, R., et al. (2021). Carbon loss from forest degradation exceeds that from deforestation in the Brazilian Amazon. Nat. Clim. Change *11*, 442–448.

56. Fan, L., Wigneron, J.P., Ciais, P., Chave, J., Brandt, M., Fensholt, R., Saatchi, S.S., Bastos, A., Al-Yaari, A., Hufkens, K., et al. (2019). Satellite-observed pantropical carbon dynamics. Native Plants *5*, 944–951.

57. Zheng, Y., Shen, R., Wang, Y., Li, X., Liu, S., Liang, S., Chen, J.M., Ju, W., Zhang, L., and Yuan, W. (2020). Improved estimate of global gross primary production for reproducing its long-term variation, 1982-2017. Earth Syst. Sci. Data *12*, 2725–2746.

58. Chen, Z., Liu, H., Xu, C., Wu, X., Liang, B., Cao, J., and Chen, D. (2021). Modeling vegetation greenness and its climate sensitivity with deep-learning technology. Ecol. Evol. *11*, 7335–7345.

59. Lefcheck, J.S. (2016). piecewiseSEM: Piecewise structural equation modelling in R for ecology, evolution, and systematics. Methods Ecol. Evol. *7*, 573–579.

60. Melillo, J.M., McGuire, A.D., Kicklighter, D.W., Moore, B., Vorosmarty, C.J., and Schloss, A.L. (1993). Global climate-change and terrestrial net primary production. Nature *363*, 234–240.

61. O'brien, R.M. (2007). A caution regarding rules of thumb for variance inflation factors. Qual. Quantity *41*, 673–690.

STAR★METHODS

KEY RESOURCES TABLE

REAGENT or RESOURCE	SOURCE	IDENTIFIER
Deposited data		
Global forest cover	MODIS Land Cover Climate Modelling Grid Product (MCD12C1)	https://lpdaac.usgs.gov/products/mcd12c1v006/
Ku-band VOD dataset	Moesinger et al. (2020)[37]	https://zenodo.org/record/2575599#.Yk57AMhBxPZ
GLASS-GPP and GLASS-LAI datasets	National Earth System Science Data Sharing Infrastructure, National Science & Technology Infrastructure of China[38,39]	http://www.geodata.cn; http://www.glass.umd.edu/Download.html
NIR-GPP dataset	Wang et al. (2021)[40]	https://figshare.com/articles/dataset/Long-term_1982-2018_global_gross_primary_production_dataset_based_on_NIRv/12981977/2
TS 4.04 Temperature and vapour pressure datasets	Climatic Research Unit	http://www.cru.uea.ac.uk/
SM and PAR of NASA Global Land Data Assimilation System (GLDAS) data products	Goddard Earth Sciences Data and Information Services Center (GES DISC)	https://disc.gsfc.nasa.gov/
Global CO_2 concentration dataset	NOAA Earth System Research Laboratory (ESRL)	https://www.esrl.noaa.gov/gmd/ccgg/trends/
Software and algorithms		
R programming language (version 4.1.2)	R Foundation, USA	https://www.r-project.org/
R package piecewiseSEM 2.1.0	Lefcheck (2016)[59]	https://www.r-project.org/

RESOURCE AVAILABILITY

Lead contact

Further information and requests for resources should be directed to and will be fulfilled by the lead contact, Prof. Hongyan Liu (lhy@urban.pku.edu.cn).

Materials availability

This study did not generate new materials.

Data and code availability

- The sources of the datasets supporting the current study will be shared by the lead contact upon request.

- This paper does not report original code.

- Any additional information required to reanalyse the data reported in this paper is available from the lead contact upon request.

METHOD DETAILS

Forest cover extraction

The global forest cover was obtained from the MODIS Land Cover Climate Modelling Grid Product (MCD12C1), adopting the classification scheme of the International Geosphere-Biosphere Programme (IGBP) (Table S1). The dataset supplies global maps of land cover at annual time steps and 0.05-degree spatial resolution for 2001 to present. Within the 17 land cover types, six forest types were determined as the research objects, including evergreen needleleaf forest (EN), evergreen broadleaf forest (EB), deciduous needleleaf forest (DN), deciduous broadleaf forest (DB), mixed forest (MI) and woody savannas (WS). In particular, woody savannas possess the maximum distribution area in global forests, covering a wide range of latitudes and climate zones. However, according to our expertise, woody savannas in the IGBP

classification scheme should be given a more accurate classification name of "woody savannas and wood-land (WS)" in this study. Considering the possible impacts of land cover change in the past decades, the change detection of time-series MCD12C1 data was conducted, and only unchanged forest areas of each type were maintained (Figure 1C).

VOD processing

Compared with other frequency bands, the observational records of the Ku-band VOD are much longer, combining various datasets from a series of passive microwave instruments.[37] Hence, we used the short wavelength Ku-band VOD (~19 GHz) product as the proxy for forest CWC and examined its spatial and temporal variations globally over the period of 1987–2017 (lasting for 31 years). The original product is available as daily global files, possessing a coarse spatial resolution of 0.25°. Furthermore, the VOD dataset was resampled to a 0.05-degree grid in accordance with the resolution of MODIS land cover data. In terms of temporal resolution, the daily files were averaged into monthly values, and then the annual maximum VOD was determined from the 12 values within each corresponding year.

GPP and LAI processing

We adopted two GPP products that were obtained with different data sources and calculation methods to strengthen the effectiveness and credibility of the conclusions. The first GPP product is the Global LAnd Surface Satellite (GLASS) dataset, obtained from the National Earth System Science Data Sharing Infrastructure, National Science & Technology Infrastructure of China (http://www.geodata.cn).[38,39] GLASS-GPP (g $C/m^2/d$) possesses a spatial resolution of 0.05° and a temporal resolution up to 8 days. Meanwhile, the GLASS-LAI product, possessing the same spatial and temporal resolution as the GPP data, was also adopted for further calculation. The second GPP product is retrieved from the satellite-based near-infrared reflectance (NIR), providing global monthly GPP estimates (g $C/m^2/d$) with a spatial resolution of 0.05°.[40]

Considering the phenology changes in most parts of the world, both variations of VOD and GPP possess phonological characteristics with the growth of forest in each year.[26,28,40,57] Correspondingly, we focused on the photosynthetic assimilation of global forests in this study, and the maximum values (peak values) could effectively reflect the carbon sequestration capacity. Hence, to give a more accurate depiction of the peak state of photosynthesis that GPP could achieve, the annual maximum GPP was served as the proxy for forest productivity. For the 12 values of NIR-GPP within each year, the maximum value was chosen as the proxy for the corresponding year. For the 8-day averaged GLASS-GPP, the monthly averaged values were first calculated to avoid possible outliers, and then the annual maximum GPP was determined from the 12 values within the corresponding year. Accordingly, the annual maximum GLASS-LAI was obtained from the original dataset.

Temperature and VPD processing

For the acquisition of time-series climate variables of forest areas, we adopted the air temperature (TMP, °C) and vapour pressure (VAP, h Pa) from the TS 4.04 dataset of the Climatic Research Unit (http://www.cru.uea.ac.uk/). In particular, the VPD was calculated as the difference between the saturated water vapour pressure (SVP, h Pa), determined by near-surface temperature, and actual water vapour pressure.[41] The annual mean TMP and VPD with a resolution of 0.05 degrees were consequently obtained.

$$SVP = 6.1121e^{\frac{17.502 \cdot TMP}{240.97 + TMP}} \qquad \text{(Equation 1)}$$

$$VPD = SVP - VAP \qquad \text{(Equation 2)}$$

SM and PAR processing

Considering the spatial and temporal coverage of SM and photosynthesis active radiation (PAR), we obtained NASA Global Land Data Assimilation System (GLDAS) data products from Goddard Earth Sciences Data and Information Services Center (GES DISC) (https://disc.gsfc.nasa.gov/). In comparison, the monthly SM and PAR data with a spatial resolution of 0.25° from the Noah-3.6 Land Surface Model were suitable for our study. The SM values (kg/m²) of different soil layers (0–10 cm, 10–40 cm and 40–100 cm) between 0 cm and 100 cm were then summed (weighted by the thickness of each layer). In addition, PAR can be obtained

from incident shortwave radiation (W/m^2).[38] The annual mean SM and PAR were resampled to 0.05 degrees in accordance with the resolution of other environmental variables.

Acquisition of CO$_2$ concentration

The global CO$_2$ concentration dataset (annual values) from the NOAA Earth System Research Laboratory (ESRL), resampled to 0.05 degrees, was used to express the CO$_2$ fertilization effect (https://www.esrl.noaa.gov/gmd/ccgg/trends/).

Conduction of MK test

For the purposes of detrending, the VOD anomaly of each month was calculated by subtracting the 31-year monthly average based on the monthly values of the VOD time series. Then, in response to the temporal autocorrelation of the time-series VOD anomaly, we conducted a trend analysis with the widely used nonparametric method, MK monotonic trend test, which possesses advantages in determining significant trends in time-series data.[42,43] For the time series (x_1, x_2, ..., x_n), the null Hypothesis H$_0$ is that there is no trend in the records, and the MK test is conducted as follows:

$$S = \sum_{k=1}^{n-1} \sum_{j=k+1}^{n} sign(x_j - x_k) \qquad \text{(Equation 3)}$$

$$sign(x_j - x_k) = \begin{cases} +1 & (x_j - x_k > 0) \\ 0 & (x_j - x_k = 0) \\ -1 & (x_j - x_k < 0) \end{cases} \qquad \text{(Equation 4)}$$

where n is the number of data points (j, $k \leq n$ and $j \neq k$) and S is a normally distributed variable that has a zero mean. When $n \leq 10$, the procedures proposed by[44] could be adopted to determine if there is a variation trend in the original time-series data. When $n > 10$, the variance of S is calculated as:

$$Var(S) = \frac{n(n-1)(2n+5) - \sum_{i=1}^{m} t_i(t_i - 1)(2t_i+5)}{18} \qquad \text{(Equation 5)}$$

$$Z = \begin{cases} \dfrac{S-1}{\sqrt{Var(s)}} & (S > 0) \\ 0 & (S = 0) \\ \dfrac{S+1}{\sqrt{Var(s)}} & (S < 0) \end{cases} \qquad \text{(Equation 6)}$$

where t_i is the number of ties for the i group, m is the number of tied groups, and Z is the statistic of the MK monotonic trend test.

A positive value of Z indicates that there is an increasing trend in the original records, and a negative Z value indicates a decreasing trend. Moreover, with a given significance level, a variation trend is considered significant when the values of Z exceed the corresponding thresholds (i.e., $\pm$ 2.32 for the 99% significance level).

Construction of SEM

SEM is a multiple regression analysis widely used to verify complex causal relationships among variables.[45] Each pathway is from the independent variable to the dependent variable, with a directional arrow for every regression model. The standard coefficients of the pathways represent the quantified effects, including positive and negative effects. The SEM in this paper was conducted using the R (version 4.1.2) package piecewiseSEM 2.1.0,[59] which could return the statistic p value, Fisher' C, Akaike information criterion (AIC) and Bayesian information criterion (BIC).

As VOD may be simultaneously regulated by climate change, the SEM contributes to removing other dominant confounding effects and making inspection and complement on the results obtained from empirical relationship between VOD and CV$_{GPP}$. For the construction of initial model, the variations of

forest CWC (represented by VOD) were mainly subject to VPD and SM. In terms of the effects on forest productivity, input variables of classical GPP conceptual model and widely used light use efficiency (LUE) models were adopted as references.[38,60] Hence, LAI was adopted as the biological variable, while environmental variables included SM, VPD, TMP, CO_2 and PAR. Furthermore, collinearity test would be conducted for all the variables with variance inflation factor (VIF).[61] As the setting of this study, the result would be considered unacceptable if any VIF value exceeded 10, and the corresponding variable should be eliminated.